Chitosan-Polyvinyl Alcohol Films Embedded Curcumin-Capped ZnO-CuO Nanoparticles: Synthesis, Characterization and Antibacterial Activity

Ahmad Fatoni[1*], Nabila Wulandari[1], Hilma Hilma[1], and Nurlisa Hidayati[2]

[1]*Pharmacy Study Program, Bhakti Pertiwi High School of Pharmacy Science, Jl. Ariodillah III No. 22, Palembang 30128, Indonesia*

[2]*Department of Chemistry, Faculty of Mathematics and Natural Sciences, Universitas Sriwijaya, Jl. Palembang Prabumulih Km. 32, Ogan Ilir 30662, Indonesia*

* ***Corresponding author:***

email: tonistifibp@gmail.com

Received: December 8, 2025
Accepted: April 8, 2026

DOI: 10.22146/ijc.114008

Abstract: *This study employs the green synthesis approach of the film chitosan-polyvinyl alcohol-curcumin-capped ZnO-CuO nanoparticles (Chi-PVA-cur-capped ZnO-CuO NPs). To create a multifunctional material, the biological and bimetallic agents work in concert to create the new chi-PVA-cur-capped ZnO-CuO NPs film.* Curcuma longa *ethanol extract was utilized to create cur-capped ZnO–CuO NPs. The casting approach was used to create this film. FTIR, XRD, SEM-EDS, and the agar diffusion method were used to examine the films for antibacterial activity. Cur-capped ZnO-CuO NPs had a particle size of 485.24 ± 5.66 nm. The swelling degree, moisture content, and thickness were all raised in all three films, but the water-soluble matter was decreased. FTIR results verified the existence of some functional groups: O–H, N–H, C–H, C=O, amide I, Zn–O, and Cu–O groups. The XRD analysis verified that all the films were amorphous. All that is present in the film is C, O, Cu, and Zn, and it has a rough form area in the SEM image. The film of type C showed a zone of inhibition in* Escherichia coli *at 20.69 ± 1.15 mm. These results imply that all-film has a great deal of promise as a strong antibacterial packaging material.*

Keywords: *chitosan; PVA; curcumin; ZnO-CuO;* Escherichia coli

■ INTRODUCTION

Nanotechnology is one of the emerging multidisciplinary subjects that is attracting a lot of attention and making a substantial contribution to the area [1]. Utilizing nanoparticles (NPs), materials with one or more dimensions smaller than 100 nm, like metal NPs, is the focus of the extremely interdisciplinary domain of nanotechnology. Both top-down and bottom-up approaches can be used to synthesize nanoparticles [2]. Metal NPs production can be carried out via physical, chemical, or biological techniques to speed up the process [3].

Turmeric ethanol extract advantages for metal oxide NPs biosynthesis include its eco-friendly nature, cost-effectiveness, and the presence of curcumin, which acts as both a reducing and capping agent to stabilize and functionalize nanoparticles. Curcumin extract can be used to biosynthesize ZnO, CuO NPs, and their combinations [4-6]. The aforementioned research indicates that curcumin extract has the capacity to operate as a stabilizing and reducing agent. As a stabilizing agent, curcumin's electrons reduce the metal from M^{x+} to M^0, and as a reducing agent, they prevent the generated NPs from aggregating arbitrarily [7]. Because combining two different metals into a single, nanostructured entity—such as core-shell or alloy—creates functionalities that surpass the sum of their individual components, bimetallic oxide NPs are selected for their superior, synergistic antibacterial effects [8-10].

Chitosan is being investigated extensively as a material in drug delivery systems [11-12], antioxidant activity [13], and antimicrobial activity [14-15]. It is claimed to have high biodegradability, high biocompatibility, and improved stability [16]. Additionally, chitosan has chemical functional groups (amino and hydroxyl groups), which make it a worthy

choice for use as a linker with curcumin, as reported by Ismail et al. [17] and used as an antibacterial. Another study conducted by Jagaiah et al. [18] showed that chitosan can be combined with metal oxide nanoparticles and can be applied in various fields. A study also conducted by Fatoni et al. [19] showed that chitosan can be combined with ZnO-CuO NPs and can be applied as an antibacterial film. The weakness of this film is that it is easily brittle.

Hydroxyl and amino groups allow for structural changes in chitosan through electrostatic interactions. Therefore, to increase the elasticity of chitosan, crosslinking with synthetic polymers that are biodegradable and biocompatible and have superior mechanical qualities, like polyvinyl alcohol (PVA), may be done [20]. According to Gutha et al. [21], PVA is a well-known substance that is highly soluble in water, non-toxic, biocompatible, hydrophilic, harmless, and non-carcinogenic. Research on the modification or customization of the desired qualities is made possible by the method of mixing chitosan with other polymers (like PVA). Blending the two polymers to create a new material with enhanced properties through the mechanism of intermolecular hydrogen bonds is one way to get over the drawbacks of using biopolymers (chitosan) and synthetic polymers (PVA) separately [18,21]. An appealing technique that has been widely employed to give chitosan new, desirable properties is the modification of chitosan through blending with PVA. This is mostly because of its ease of use, efficacy for real-world applications, and accessibility of a large variety of natural and synthetic polymers for blending [22].

Because they create a biocompatible, biodegradable, and mechanically improved composite, chitosan and PVA are employed combined as flexible supporting materials, especially in biomedical, packaging, and environmental applications. PVA offers superior film-forming, mechanical strength, and flexibility, whereas chitosan delivers natural bioactivity (antibacterial) [23-24]. The main weakness of blending chitosan and PVA for antibacterial properties is that the resulting blend may have weak intrinsic antibacterial activity on its own, often requiring additional components like metal oxide nanoparticles [25].

The addition of TiO_2 NPs to a mixture of chitosan and PVA can be used for wound healing [26]. A study by Kishore et al. [27] showed that chitosan and PVA can be used as supporting materials in the process of making chitosan-PVA-ZnO-Cu NPs films, and the film is used as an antibacterial and photocatalytic dye degradation. Enhancing chitosan as an antibacterial agent involves modifications like incorporating other components, such as metal NPs. These enhancements can increase its positive charge density, improve solubility, and create synergistic effects, leading to a wider antibacterial spectrum and stronger efficacy against bacteria. To overcome the above, the concentration of metal oxide NPs was reduced, and the concentration of chitosan was increased, so it is necessary to modify the results of previous research conducted by Fatoni et al. [19].

The previous research [28-29] stated that a combination of curcumin, chitosan, and PVA can be used as an antibacterial and wound healing agent. As explained by Khezri et al. [30], there are hydrogen bonds (intermolecular) formed between the chemical structures of curcumin and chitosan. Due to its dual function as a stabilizing (capping) and reducing agent, curcumin capping is essential in green synthesis since it produces stable, biocompatible NPs without the use of hazardous chemicals [7,31].

To improve the antibacterial activity of a chitosan-PVA nanomaterial against *Escherichia coli* by adding cur-capped ZnO-CuO NPs, we combined chitosan with PVA and added cur-capped ZnO-CuO NPs to the chitosan-PVA. The initial biosynthesis of the nanomaterial curcumin-capped ZnO-CuO involved combining an ethanolic solution of curcumin, copper sulfate, and zinc acetate. Blending a chitosan-PVA solution using intermolecular hydrogen bonds and hydrophobic side chain aggregation, then adding the cur-capped ZnO-CuO NPs to the chitosan-PVA mixture.

■ EXPERIMENTAL SECTION

Materials

These consist of glacial acetic acid, zinc acetate pentahydrate, copper sulfate pentahydrate, sodium hydroxide, PVA, ethanol, and nutritious agar, except

chitosan (DD 87%). All materials were purchased from Merck. In our lab, we use *Escherichia coli* ATCC 8739 microorganisms, including aquadest. *Curcuma longa* from Palembang city.

Instrumentation

Physical structure and crystallinity size measurement were carried out using X-ray diffraction (Shimadzu XRD 6000). Surface morphology analysis was carried out using scanning electron microscopy (Axia ChemiSEM, Thermo Fisher Scientific). Shimadzu Prestige-21 FTIR spectrophotometer for functional group analysis. The size and size distribution of particles are ascertained using a particle size analyzer (Bettersizer S3 Plus, Bettersize Instruments). Thermo Scientific's Genesys 150 UV-vis spectroscopy is a useful method for describing cur-capped ZnO-CuO NPs.

Procedure

Preparation of C. longa *ethanolic extract as medium for biosynthesis*

In summary, a freshly grated turmeric (*C. longa*) (25 g) is placed in a maceration bottle with ethanol 96%, v/v (250 mL) and allowed to maceration process (48 h). After 48 h, the solution was filtered to separate the solid substance from the extract solution, creating the first macerate. The solution was filtered to yield macerate II after the solid material was macerated again for 48 h using 250 mL of 96% v/v ethanol. Macerates I and II are combined for use in the biosynthetic process.

Phytosynthesis of curcumin-capped zinc oxide-copper oxide nanoparticles (cur-capped ZnO-CuO NPs)

This procedure is based on previous research with a few small modifications [32-34]. The solutions of copper sulfate (0.1 M, 100 mL) and zinc acetate (0.1 M, 100 mL) are mixed with 200 mL of *C. longa* ethanolic extract in a 500 mL beaker. Then, for an hour at room temperature, the mixture was continuously stirred. NaOH solution (0.8 M) was added to the mixture to bring its pH up to 9. Then, with constant stirring, the entire mixture was heated to 80 °C. For one night, the leftover mixture was left to precipitate at room temperature. After thoroughly cleaning the precipitate (cur-capped ZnO-CuO NPs) with distilled water and a 96% v/v ethanol solution, it was dried in a vacuum oven set at 80 °C until it became charred. In the end, cur-capped ZnO-CuO NPs were calcined dry (muffle furnace, 400 °C) for 2 h.

Fabrication of chitosan-PVA-curcumin-capped zinc oxide-copper oxide nanoparticles film (chit-PVA-cur-capped ZnO-CuO NPs)

The film was made using the method described in our previous study [19] with slight modifications. To make a 0.5 g chitosan solution, 15 mL of a 2.5% v/v aqueous acetic acid solution was added to a 250 mL glass beaker. Following that, the liquid was constantly stirred to produce a homogenous solution using a hotplate set at 25 °C with a stirring rate of 100 rpm. The mixture was then continuously stirred for 1 h at 25 °C (100 rpm) while 0.05 g of cur-capped ZnO-CuO NPs was added to 15 mL of the chitosan solution above. Finally, the mixture was spun continuously for 30 min at 25 °C (100 rpm) while being combined with 10 mL of the 2.5% (w/v) PVA solution. The resulting solution was then evenly distributed on a petri dish and allowed to dry at ambient temperature. The film was completely dry and usable after 7 d. As shown in Table 1, the other films were made for different comparisons.

Properties of films (chit-PVA-cur-capped ZnO-CuO NPs A, B and C)

Film thickness. The film thickness was measured at three points using a digital clipper. The average value was determined after each film was measured three times [35-36].

Table 1. Materials required for the synthesis of chit-PVA-cur-capped ZnO-CuO NPs films

No	Chitosan (g)	Cur-capped ZnO-CuO NPs (g)	Polyvinyl alcohol solution 2.5% w/v (mL)	Film type
1	0.5	0.05	10	A
2	0.5	0.10	10	B
3	0.5	0.15	10	C

Content of moisture (MC). Using Eq. (1), the moisture content was determined. Following a 3-hour oven drying phase at 105 °C, the film's initial weight (W_1), which measured 2 cm by 2 cm, was recorded, and its final weight (W_2) was ascertained [36].

$$MC(\%) = \frac{W_1 - W_2}{W_2} \times 100\% \quad (1)$$

Solubility in water. To determine how much of the film's components could be leached by water, the film's solubility in water was computed. We used the oven drying method (105 °C, 3 h) to determine the W_1 of the film (2 cm × 2 cm). After cooling, the material was left to soak for 24 h at room temperature in 10 mL of distilled water. The W_2 was noted when the film was taken out and dried for 3 h at 105 °C [35-36]. Using Eq. (2), the solubility of the film was determined.

$$\text{Water Soluble Matter}(\%) = \frac{W_1 - W_2}{W_1} \times 100\% \quad (2)$$

Swelling degree (SD). After being divided into 2×2 cm^2, the films were dried in an oven set to 110 °C until they reached a constant weight. Following a 24-hour soaking in distilled water at room temperature, the dry film sections were wiped using paper towels to remove any leftover surface water, and the wet weight of the films was measured (W_1). After that, the swollen films were dried once again at 110 °C in an oven until they acquired a consistent weight (W_2), and the weight was once more documented [35]. Using Eq. (3), the swelling degree of the film was determined.

$$SD(\%) = \frac{W_1 - W_2}{W_2} \times 100\% \quad (3)$$

Biological activity of film

E. coli was the test bacterial strain used to evaluate the produced nanoparticles' antibacterial properties. The inoculum suspension was made by introducing a sterile 0.9% NaCl solution into a fresh culture, shaking it, and keeping an eye on the optical density at 580 nm, adjusting it until the inoculum's transmittance reached 25% [37], equivalent to 1×10^8 CFU/mL. After the microbial inoculum had solidified in 10 mL of nutritional agar (the first layer), it was inoculated into the second layer of the petri plate using the agar diffusion method. All films and comparators (chitosan film, PVA film, and chloramphenicol) were placed on the second layer. Each film has a diameter of ± 6 mm. The plate was incubated at 37 °C for 24 h. Lastly, a caliper was used to quantify the zone of inhibition in millimeters, which was then compared to the standard chloramphenicol. The film's ability to effectively stop bacterial growth is demonstrated by the greatest inhibition zone.

■ RESULTS AND DISCUSSION

Proposed Chemical Reaction for The Formation of Cur-capped ZnO-CuO NPs and chit-PVA-cur-capped ZnO-CuO NPs Films

The polyphenols (from curcumin) and zinc acetate or copper sulfate (precursor) may react to generate an intermediate product (zinc or copper hydroxide), which could be the chemical reaction for the phytosynthesis of ZnO or CuO nanoparticles. The following reactions demonstrate that this chemical is subsequently transformed into either CuO or ZnO by the heat produced during the drying step [38].

$$Zn(CH_3CO_2)_{2(aq)} + 2R-OH \rightarrow Zn(OH)_{2(s)} + 2R-CH_3CO_{2(aq)} \quad (4)$$

$$Zn(OH)_{2(s)} + \text{heat} \rightarrow ZnO_{(s)} + H_2O_{(v)} \quad (5)$$

$$CuSO_{4(aq)} + 2R-OH_{(aq)} \rightarrow Cu(OH)_2 + R_2-SO_{4(aq)} \quad (6)$$

$$Cu(OH)_{2(s)} + \text{heat} \rightarrow CuO_{(s)} + H_2O_{(v)} \quad (7)$$

According to the following processes, curcumin's phenolic hydroxyl groups donate electrons to their respective metallic ions (ZnO and CuO) by acting as reducing agents for divalent metals (Zn^{2+} and Cu^{2+}) ions [39].

$$Cu^{2+} + C_{14}H_{14}O_4 \rightarrow CuO + CO_2 + H_2O + \text{other byproducts} \quad (8)$$

$$Zn^{2+} + C_{14}H_{14}O_4 \rightarrow ZnO + CO_2 + H_2O + \text{other byproducts} \quad (9)$$

Using curcumin as a stabilizing and reducing agent first caused the metal ions to be reduced, and then the enol form stabilized the produced NPs on their surface [4,7]. According to research findings by Moussawi and Patra [40], curcumin mostly exists in the enol form because its spectra did not exhibit any peaks in the carbonyl range (1800–1650 cm^{-1}), either in the solid state or in solutions. In the 1:1, 2:1, or 3:1 curcumin:

metal combination, the enol form functions as a great chelator by binding with the metal ion, allowing the metal ion to stoichiometrically replace the enolic proton [7,41-42] as seen in Fig. 1. Fig. 2 shows the product of cur-capped ZnO-CuO NPs. PVA's hydroxyl (–OH) groups and chitosan's amino groups (NH_2) can create hydrogen bonds (intermolecular) as both hydrophilic polymers [43-45]. The hydroxyl groups of the glucosamine unit of chitosan and curcumin may interact via forming intermolecular hydrogen bonds [14,30,46], as illustrated in Fig. 3. Digital photo of all chit-PVA-cur-capped ZnO-CuO NPs films can be seen in Fig. 4.

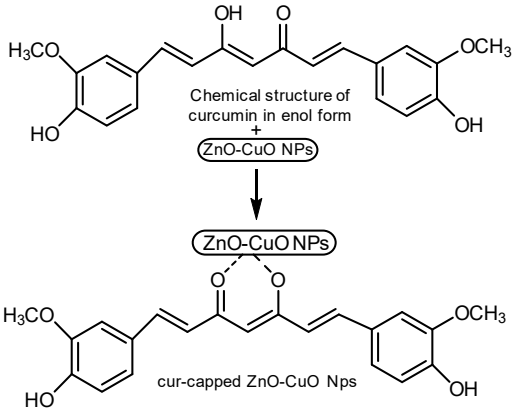

Fig 1. Reaction between ZnO-CuO NPs and curcumin

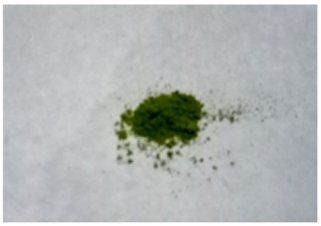

Fig 2. Photographs of the product cur-capped ZnO-CuO NPs

The Properties of Films

The thickness (mm), moisture content (%), water soluble matter (%) and swelling degree (%) of the films are the parameters studied and can be seen in Table 2. The results show that the addition of cur-capped ZnO-CuO NPs increased the thickness of the films, and the effects became more pronounced as the amount of cur-capped

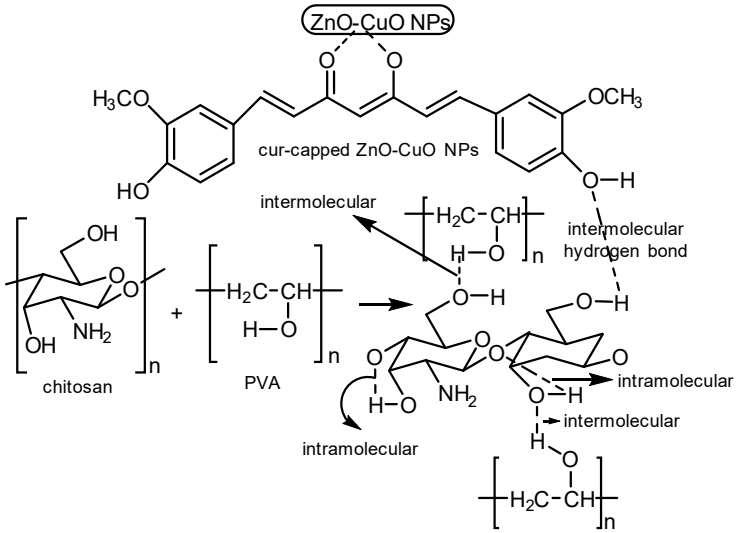

Fig 3. The proposed chemical reaction mechanism that occurs in the film

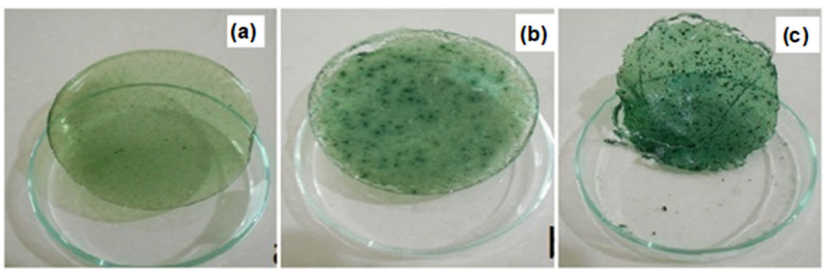

Fig 4. Photograph of chit-PVA-cur-capped ZnO-CuO NPs film (a) type A, (b) type B, and (c) type C

Table 2. The properties of films

Type of films	Thickness (mm)*	Moisture content (%)*	Water soluble matter (%)*	Swelling degree (%)*
A	0.17 ± 0.04	9.09 ± 0.01	50.00 ± 0.82	140.00 ± 0.62
B	0.20 ± 0.03	10.00 ± 0.08	28.57 ± 0.20	233.33 ± 0.48
C	0.30 ± 0.09	9.09 ± 0.01	20.00 ± 0.82	200.00 ± 0.82

* Mean ± Standard Deviation (SD) is used to express values

ZnO-CuO NPs was increased. According to studies by Ahmad and Sarbon [47] and Dordevic et al. [48], the inclusion of solid nanoparticles thickened the film.

The pure chitosan film had a high moisture content (38.22%), according to literature [35]. Through hydrophilic interactions like hydrogen bonds, the numerous hydrophilic groups (–OH and $–NH_2$) in the chitosan molecules were able to absorb and hold a comparatively large amount of water in the pure chitosan film [35]. When PVA and ZnO-CuO NPs capped with curcumin were added, the moisture content dropped. The interactions between cur-capped ZnO-CuO NPs and PVA and chitosan may be the cause of these outcomes. According to the study, when metal oxide NPs are added to a chitosan-PVA matrix, the resulting film is thicker than when the polymers are just combined. This happens because adding NPs raises the total solid content in the polymer matrix. This could be because the NPs and polymers form hydrogen bonds (H···O interactions), which impede the movement of the polymer chain [25].

The amino groups (NH_2) included in the chitosan polymer can easily be protonated to produce an ammonium group (NH_3^+) in an acidic solution (acetic acid). It becomes more soluble in water as a result. In contrast, the PVA polymer has a large number of hydroxyl groups that form hydrogen bonds with water molecules, which makes it very soluble in aqueous solutions. As a result, the chitosan-PVA polymer can swell more easily in aqueous conditions [49].

The interaction between the polar groups and the water molecules determines how much the polymer swells in the aqueous medium. A longer immersion period makes it easier for water molecules to diffuse into the polymer segments, which leads to the formation of hydrogen bonds between several polar groups and the water molecules [49]. In terms of solubility, the addition of cur-capped ZnO-CuO NPs caused an increase in values in films with the increasing NPs concentration (cur-capped ZnO-CuO NPs). The result shows that the addition of cur-capped ZnO-CuO NPs increases the swelling degree with increasing concentration of cur-capped ZnO-CuO NPs [48].

Cur-capped ZnO-CuO NPs were added, the films' water content either barely altered or went down. Based on the findings, the solubility values decreased when cur-capped ZnO-CuO NPs was added [48]. There can be fewer water molecules because of the hydrogen bond interactions between the film molecules and the hydroxyl groups (chitosan) on the surface of cur-capped ZnO-CuO NPs. This is because some of the initial hydrogen-bond interactions between the packaging matrix and water molecules can be transferred [48].

Optical Properties

Fig. 5 shows UV-vis spectra of Cu^{2+} solution, Zn^{2+} solution, ethanolic extract of *C. longa*, and cur-capped ZnO-CuO NPs at room temperature in the range 200–1000 nm. As seen in Fig. 5(a), Cu^{2+} solution has a maximum band at 805 nm [50]. The *d-d* transitions of the d^9 electronic structure, which are influenced by the Jahn-Teller effect, cause the Cu^{2+} solution to exhibit a maximum absorption band, which is often stated to be between 740 and 880 nm [51].

The Zn^{2+} solution shows a band at 218 nm and below 250 nm [52] (Fig. 5(b)). In Zn^{2+} solutions, the 218 nm absorption band is mainly linked to ligand-to-metal charge transfer (LMCT) or charge-transfer transitions between the zinc ion and its coordinating ligands (such as water) rather than *d-d* transitions [53-54]. Ethanolic extract of *C. longa* shows a band maximum at 436 nm (Fig. 5(c)) because of the π-π* type excitation resulting from the electronic dipole [17,55-56]. Cur-capped ZnO-CuO NPs showed a characteristic feature at 460 nm (Fig. 5(d)), indicating the formation of

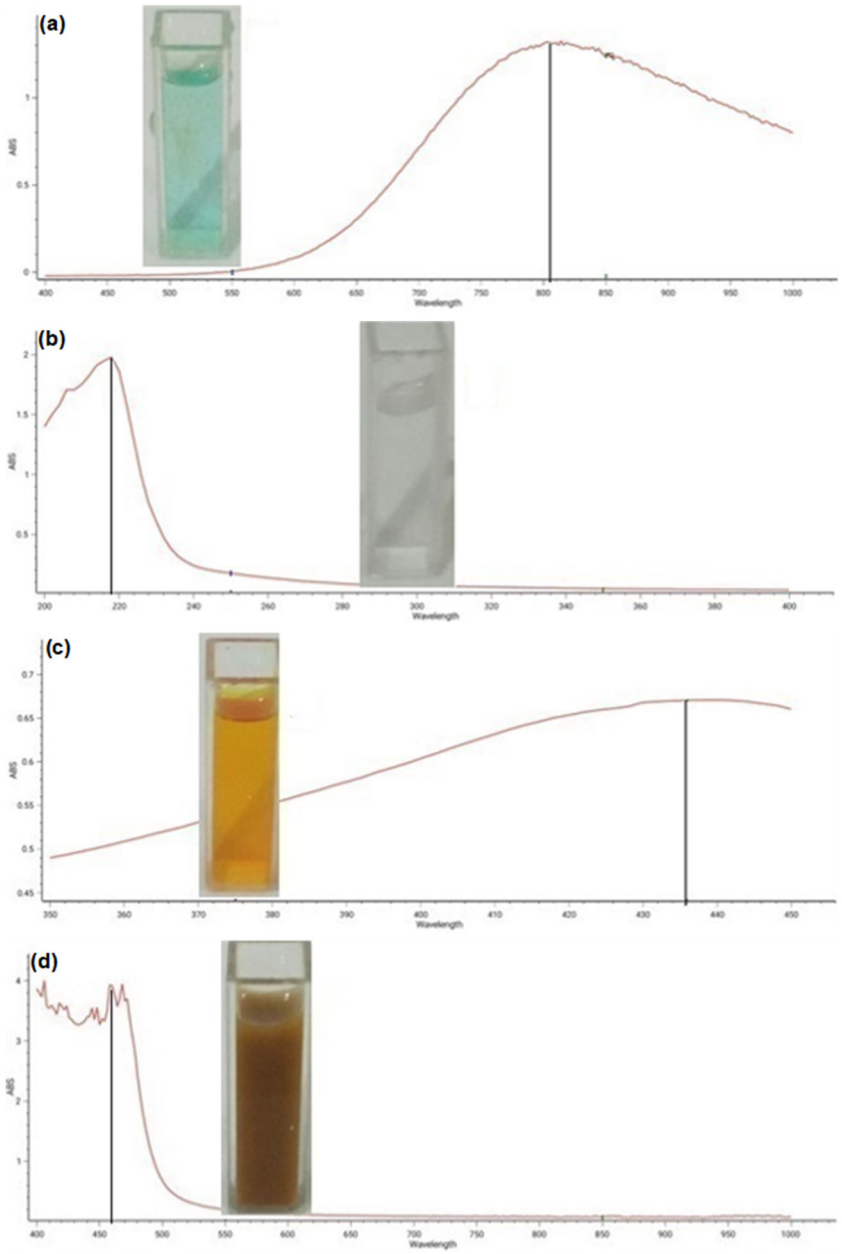

Fig 5. UV-vis spectra of (a) Cu^{2+} and (b) Zn^{2+} solution, (c) ethanolic extract of *C. longa* and (d) cur-capped ZnO-CuO NPs

ZnO-CuO NPs capped with curcumin extract [32,57].

Particle Size and Polydispersity Index Analysis

Size and polydispersity index of cur-capped ZnO-CuO NPs as seen in Fig. 6. Cur-capped ZnO-CuO NPs were found to have a homogeneous particle size of 485.24 ± 5.66 nm (Fig. 6) and a polydispersity index of 0.688 ± 0.540 due to the complexation with ZnO-CuO nanoparticles [58]. Particle aggregation and the presence of curcumin molecules on the NPs surface [38] are likely the causes of this size decrease of cur-capped ZnO-CuO NPs. Particle size aggregation, primarily caused by the electrostatic attraction of ZnO-CuO nanoparticles, is primarily responsible for the wide particle size distribution and polydispersity index [38]. The research results from El-Kattan et al. [57] and Saif et al. [59] also showed that the particle size of curcumin-metal oxide NPs was greater than 100 nm. This is possible, in accordance with

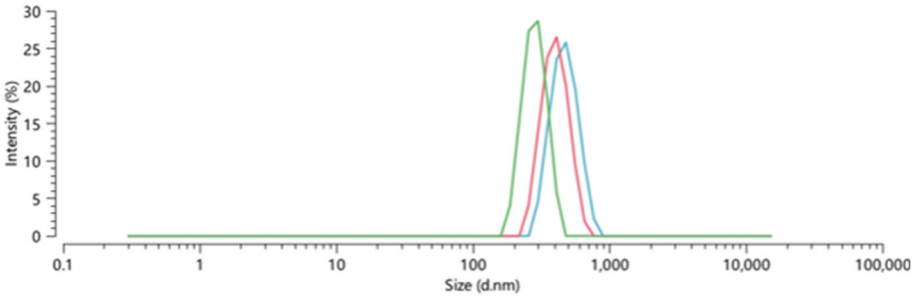

Fig 6. The results of particle size analysis from cur-capped ZnO-CuO NPs

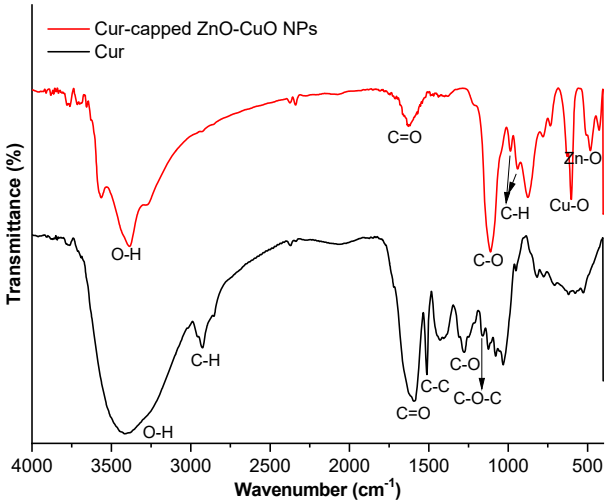

Fig 7. FTIR spectrum of cur. and cur-capped ZnO-CuO NPs

their aggregation, the as-prepared NPs' hydrodynamic particle size is larger. Their hydrophilicity is the reason for this aggregation. Furthermore, forming a layer of water surrounding the material increases the strength of the steric forces of the functional groups on the NPs' surface [57].

FTIR Analysis

Cur-capped ZnO-CuO NPs

FTIR spectra of curcumin and cur-capped ZnO-CuO NPs as seen in Fig. 7. Curcumin's FTIR spectra (Fig. 7) showed a predictable band around 3415 cm^{-1}, which is attributed to the stretching vibration (ν) of the phenolic –OH bond. The bending vibration (δ) of the C–H group attached to the curcumin's benzene ring is represented by the peak at 1429 cm^{-1}, and the ν(C=O) was associated with the absorption peak at 1593 cm^{-1} [60].

The FTIR spectrum of curcumin showed absorption peaks of aromatic ν(C–O), ν(C–O–C) and ν(C–C) vibrations at 1512, 1276, and 1159 cm^{-1} [60-62]. C–O–C from methoxy groups is responsible for the peak at 1031 cm^{-1} [62]. As previously observed, neither in the solid state nor in solutions did the curcumin spectra exhibit any peak in the carbonyl region (1800–1650 cm^{-1}), suggesting that curcumin is mostly found in the enol form [40].

Cur-capped ZnO-CuO NPs (Fig. 7) FTIR analysis revealed the presence of characteristic absorption bands at 3562–3385 and 1635 cm^{-1} due to –OH intermolecular bonding of alcohol and ν(C=O), respectively [39,59-60]. However, the curcumin-capped ZnO-CuO NPs' C=O peak at 1593 cm^{-1} is shifted to 1635 cm^{-1}, possibly as a result of the charge-transfer interaction between the curcumin C=O group and ZnO-CuO NPs [60].

The δ(C–H) and ν(C–O) of the pluronics on the NPs surface may be responsible for the peaks at 1111 and 985–941 cm^{-1} [60]. Cur-capped ZnO-CuO NPs has a peak at 875 cm^{-1}, which is attributed to ν(C–O) [63]. Qasem et al. [64] stated that the peak in the 500–700 cm^{-1} range should be of ν(Cu–O) and emerged at 603 cm^{-1}. Peak at 482–426 cm^{-1} showed a significant absorption peak in the 400–500 cm^{-1} range, which was attributed to the Zn–O bond's distinctive stretching vibration [65].

The film of chit-PVA-cur-capped ZnO-CuO NPs

FTIR spectrum of chit-PVA-cur-capped ZnO-CuO NPs films and their constituent materials are shown in Fig. 8 and 9. Fig. 8, according to Zidan et al. [66], the broadband at roughly 3410 cm^{-1} is attributed to the stretching vibration of PVA's O–H group. Around 2941 cm^{-1} is where the band corresponding to the ν(as) CH_2 is visible. The ν(C=O) and ν(C=C) modes have been assigned to the peaks at 1720 and 1658 cm^{-1}, respectively. Symmetric bending of CH_2 has been identified as the cause

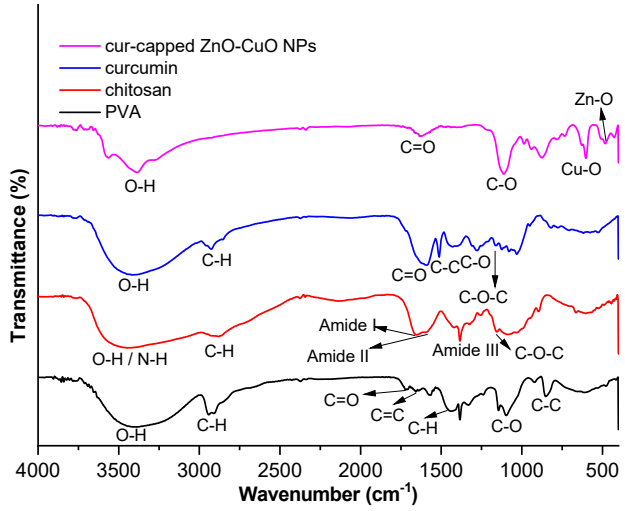

Fig 8. FTIR spectra of cur-capped ZnO-CuO NPs and their reference materials

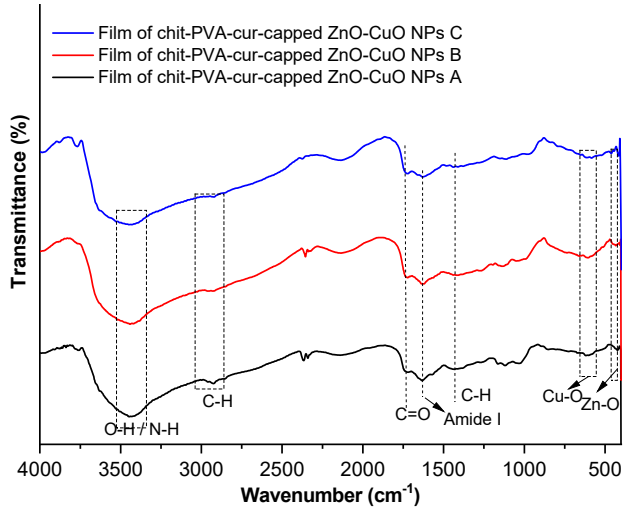

Fig 9. FTIR spectra of chit-PVA-cur-capped ZnO-CuO NPs films

of the absorption band at 1438 cm^{-1}. The ν(C–O) of the C=O groups in the PVA backbone is represented by the band at roughly 1097 cm^{-1}. At 850 cm^{-1}, moderate absorption from the planar zigzag carbon backbone's C–C stretching vibrations is detected. The wagging mode of OH groups is attributed to the peak at 615 cm^{-1}, whereas CH_2 rocking is assigned to the peak at 920 cm^{-1}, and δ (CH+OH) is assigned to the peak at 1330 cm^{-1}.

According to earlier research [67-68], in chitosan, the band at about 3448 cm^{-1} is the axial of the O–H group stretch superimposed on the nitrogen-hydrogen bond stretch band. The amide I (O=C–NHR) characteristic band at 2920–2881 cm^{-1} in the 1654 cm^{-1} area is brought on by the asymmetric stretch of the C–H group. The protonated amine group's (NH_3^+) vibrational deformation is indicated by the band at 1598 cm^{-1} (amide II, amine-NH_2). The band at 1382 cm^{-1} is the result of amino groups deforming axially to CN. However, it appears that the characteristic bands of the saccharide structure (the C–O–C glycosidic link) are located at approximately 1153 cm^{-1}. The pyramided rings' C–O–C stretching is linked to the strong band at 1078–1033 cm^{-1}.

A broad band at 3100–3500 cm^{-1} (3448, 3441, and 3446 cm^{-1}) in the FTIR spectra of films A, B, and C (Fig. 9) indicates the ν(OH) and may overlap with the N–H bands of amide and amine [43]. The ν(s) C–H group is represented by the bands at 2922, 2931, and 2924 cm^{-1} [69]. The remaining C=O acetate groups from PVA vibrate at 1724, 1722, and 1722 cm^{-1} [43,69]. The interaction between the O–H and δ NH of PVA and chitosan is responsible for the peaks at 1629, 1625, and 1633 cm^{-1} [43]. The δ C–H group may be seen at 1438, 1409, and 1435 cm^{-1} [43].

The crystalline portion of PVA, represented by the ν(C–O), is seen as a shoulder at 1112, 1130, and 1163 cm^{-1}, while the amorphous portion, represented by the ν(C=O), is seen at 979, 1049, and 1029 cm^{-1} [69]. Previous studies have revealed that the peak for the Cu–O group is 584, 603, and 619 cm^{-1} [64]. The ν(Zn–O) group is responsible for the peaks located at 425–475, 422–452, and 424 cm^{-1} [65]. Peak shifts brought on by interactions between two or more polymer mixes via hydrogen bonding are visible in the FTIR spectra. Intramolecular hydrogen bonding between the O–H group (PVA) and the O–H and –NH_2 groups (chitosan) may be the cause of an increase in peak intensity [70].

XRD Analysis

Curcumin's distinctive reflections may be seen at 2θ = 25.3° and 29.82° in the diffractogram of the cur-capped ZnO NPs [71], as illustrated in Fig. 10. The diffractogram of curcumin was found at 2θ = 13.58°, 22.71°, 24.57°, 25.19°, 27.32°, and 29.71° in cur-capped CuO NPs [72-74], while curcumin's diffractogram of

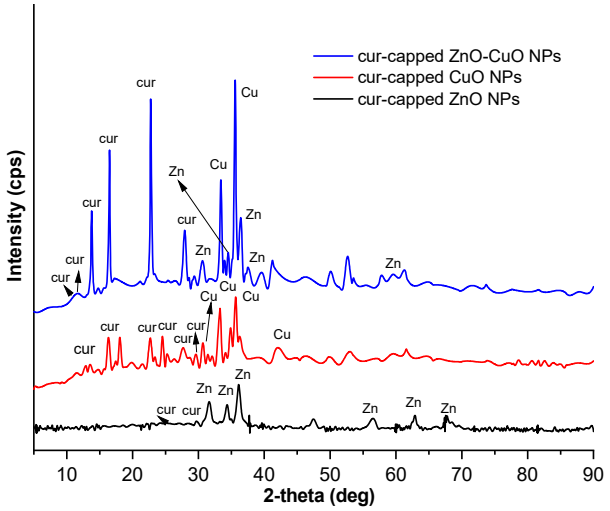

Fig 10. Diffractogram of cur-capped ZnO, cur-capped CuO and cur-capped ZnO-CuO NPs

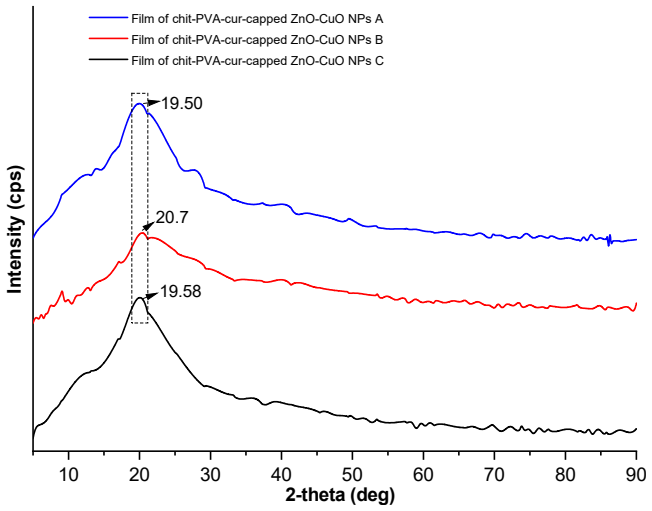

Fig 11. XRD pattern of chit-PVA-cur-capped ZnO-CuO NPs film A, B and C

cur-capped ZnO-CuO NPs was found at 13.78°, 14.86°, 17.41°, 22.75°, and 27.82° [72-74].

Significant diffraction peaks are observed at 31.70°, 34.38°, 36.13°, 56.34°, 62.32°, and 67.66° in the ZnO nanoparticles' XRD investigation [60,75-76]. The presence of CuO NPs is confirmed by the 2θ peaks seen at 31.29°, 33.24°, 35.62°, and 42.36° [77-78]. Fig. 10 displays the ZnO-CuO NPs' XRD patterns. According to Varaprasad et al. [79], the CuO NPs exhibited distinct primary intensity peaks at 2θ = 33.37° and 35.53°. The primary peaks of ZnO NPs are 2θ at 30.72°, 34.52°, 36.37°, 37.55°, and 60.28° [60,80-81]. According to Sathiyabama et al. [82], the XRD pattern of cur-Cu NPs has a crystalline nature and the production of a polycrystalline, two-phase nanocomposite is usually confirmed by the XRD pattern of ZnO-CuO NPs [83].

The crystallite size of nanoparticles is calculated using Debye Scherrer's formula [84], as shown in Eq. 10.

$$D = (0.9 \times \lambda) / (\beta \times \cos\theta) \quad (10)$$

The symbols D, λ, β, and θ respectively represent the crystallite size (nm), Bragg's angle, full width at half maximum (FWHM), and the wavelength of the used X-ray. It was estimated that the cur-capped ZnO-CuO NPs had a crystallite size of 5.72 nm.

Fig. 11 displays the diffractogram of film types A, B, and C. Despite the addition of cur-capped ZnO-CuO NPs, these three types of films share the same characteristics. The diffractogram of film types A, B, and C (Fig. 11) does not show the distinct signals of cur-capped ZnO-CuO NPs, suggesting that the addition of a trace amount of cur-capped ZnO-CuO NPs to the chitosan-PVA matrix changed its properties. There are peaks at about 2θ = 19.58°, 20.7°, and 19.50° for film types A, B, and C, respectively. The film types A, B, and C's diffractogram revealed comparable diffraction at 2θ in the 19.50°–20.7° range. This peak demonstrates the film's amorphous nature. The amorphous nature implies that the O–H and N–H groups of the PVA and chitosan interacted (intermolecular and intramolecular hydrogen bond lengths) to produce the amorphous structure of the film [16,78,85].

The low percentage of NPs is the cause of the lack of distinctive peaks, not the deterioration of NPs crystallinity [25]. The absence of crystalline morphology of cur-capped ZnO-CuO NPs, as a uniform dispersion of metal oxide NPs in this film via hydrogen bonding or electrostatic forces of attraction [86], is confirmed by the diffractogram of the chit-PVA-cur-capped ZnO-CuO NPs.

SEM/EDS Analysis

SEM/EDS studies were carried out to obtain the morphology and elemental concentration of cur-capped ZnO-CuO NPs developed as shown in Fig. 12 and 13. Table 3 displays the composition of elements analyzed

using SEM/EDS. According to the results, the produced cur-capped ZnO-CuO NPs' elemental composition (atomic percent) was as follows: 52.6% oxygen, 24.6% carbon, 16.4% Cu, and 2% Zn (Table 3). Fig. 12 and 13 illustrates the full conjugation process between Zn or Cu and curcumin based on the EDS and FTIR data [87].

Using elemental mapping, the dispersion of the cur-capped ZnO-CuO NPs was seen (Fig. 14). On the surface of the cur-capped ZnO-CuO NPs, the constituent elements C (red) and O (green) are derived from curcumin, while Zn (black) and Cu (blue) are derived from ZnO and CuO NPs, respectively. Fig. 15 depicts the surface structure of film types A, B, and C. Surface morphological variations are seen in SEM micrographs. The rough areas of every film were noted, as displayed in Fig. 15(a–c). The chitosan molecules cause the PVA matrix's compact structure to be disrupted, which results in roughness [88]. The blend surface is showing white spots in Fig. 15, and the cur-capped ZnO-CuO NPs are visible as rounded nanostructures embedded in a chitosan-PVA surface.

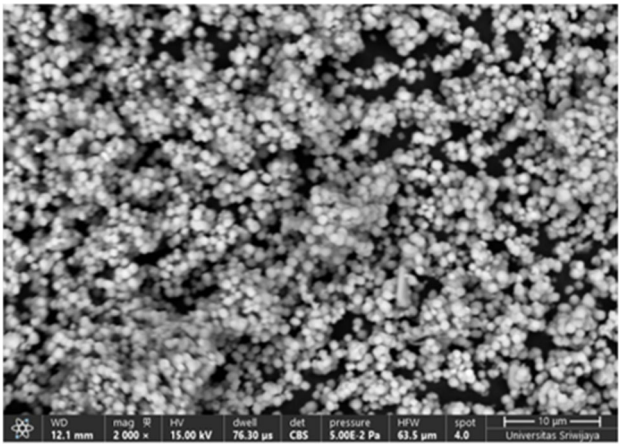

Fig 12. The surface morphology of cur-capped ZnO-CuO NPs

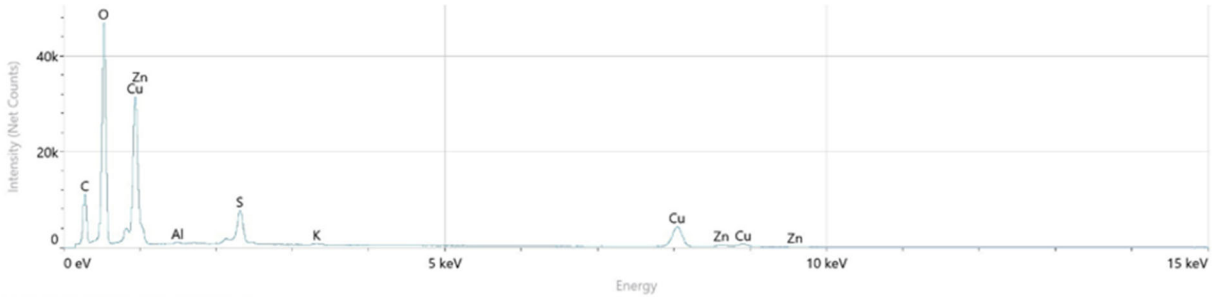

Fig 13. SEM-EDS spectrum of cur-capped ZnO-CuO NPs

Table 3. Percentage of constituent atoms

Material	Element (%)						
	C	O	Al	S	K	Cu	Zn
Chit-PVA-cur-capped-ZnO-CuO NPs	24.26	52.60	0.20	3.70	0.20	16.70	2.00

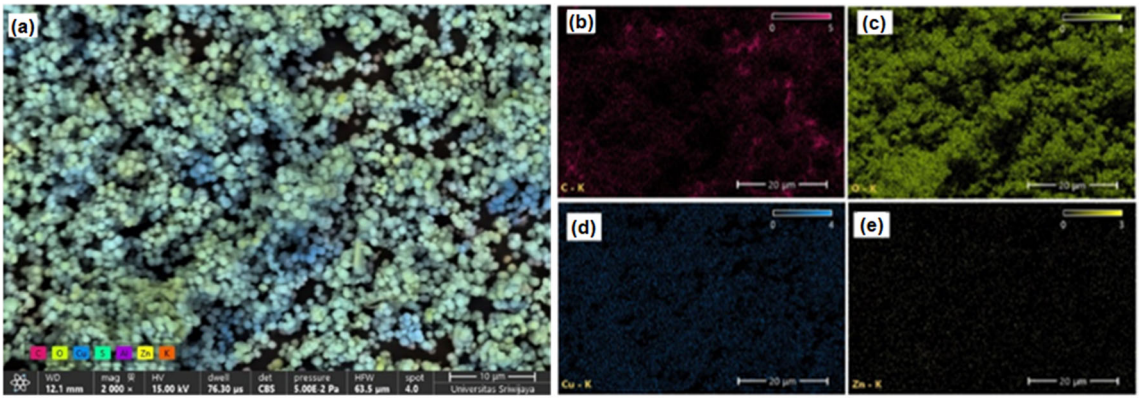

Fig 14. SEM-mapping images of cur-capped ZnO-CuO NPs (a) overall element, (b) C, (c) O, (d) Cu, and (e) Zn

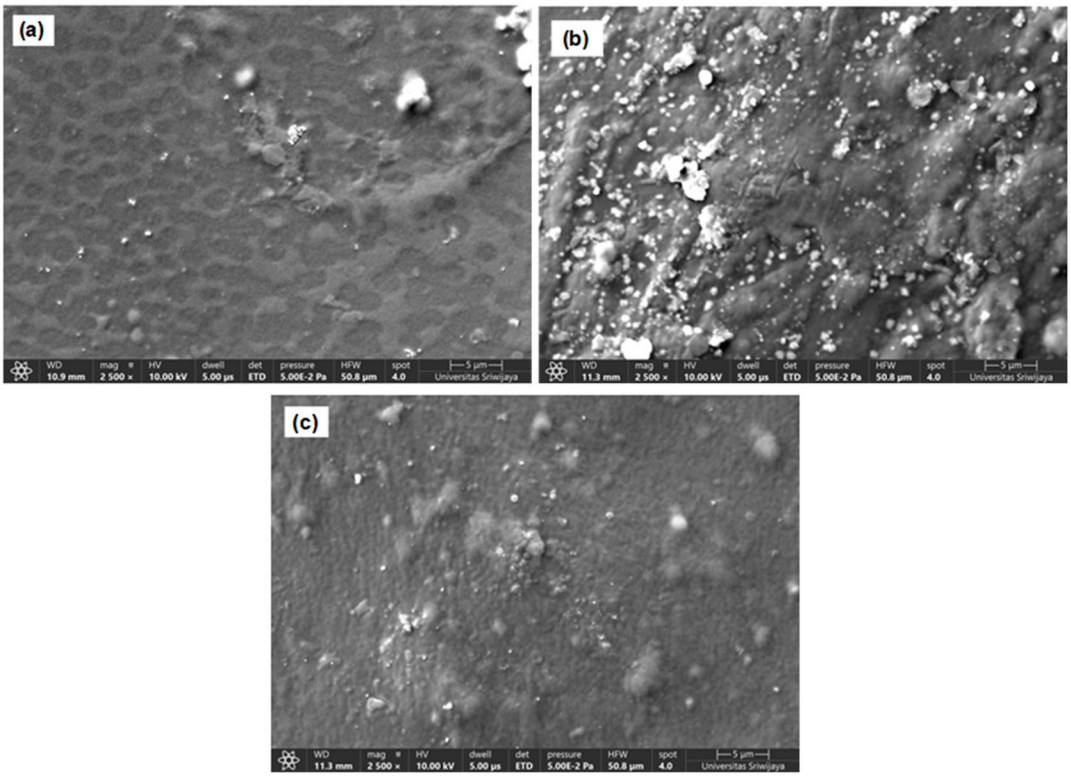

Fig 15. Surface structure of films (a) A, (b) B, and (c) C observed by SEM at a magnification of 2,500×

Antibacterial Study

The antibacterial effectiveness of each film under examination is depicted in Fig. 16. Fig. 16 shows the zones of inhibition for each film as well as the average zone of inhibition for each sample for each of the three replicates. Film C has a greater average inhibition zone than films A and B, as seen in Table 4 and Fig. 16. Chitosan and bimetallic nanoparticles (ZnO-CuO NPs) were added to film C to enhance its antibacterial capabilities against *E. coli*.

Pure PVA films (D) did not exhibit antibacterial, according to the results [89-90]. Naturally, a pure PVA film lacked the ability to inhibit both Gram-positive and Gram-negative bacteria [89,91-92]. This is due to the fact that pure PVA film typically lacks intrinsic antibacterial qualities [89] and PVA's chemical structure, which is mainly made up of O–H groups, does not automatically alter the structures of bacteria or obstruct their metabolic functions in order to prevent growth.

Surface-surface interactions between the biopolymer chains and microbial cell walls have been implicated in chitosan's antibacterial properties [93-94]. Bacteria sticking to the chitosan films [95], as seen in Fig. 16, indicate that the chitosan chains in the films (E) used

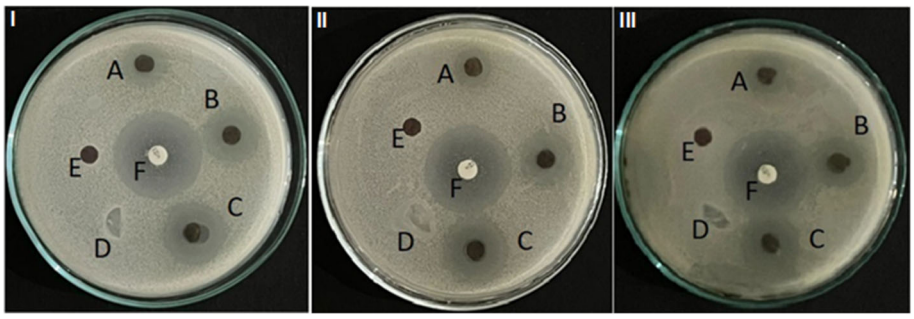

Fig 16. Antibacterial activity test of *E. coli* bacteria on all films

Table 4. *E. coli* antimicrobial evaluation results for each film

Petri dish	Inhibition zone (mm) of film					
	A (A)	B (B)	C (C)	PVA (D)	Chitosan (E)	Chloramphenicol (0.1 % w/v, F)
I	13.62	18.28	20.94	0.00	0.00	28.31
II	12.08	17.35	21.69	0.00	0.00	28.02
III	12.91	15.42	19.43	0.00	0.00	28.01
Average ± SD	12.87 ± 0.77	17.02 ± 1.46	20.69 ± 1.15	0.00	0.00	28.11 ± 0.17

here did not interact with the microbial cell walls and, hence, did not exhibit any bactericidal properties. This proved that chitosan cannot permeate the surrounding agar and that its biocidal action is associated with the release of protonated glucosamine fractions into the culture media [96]. A previous work [97] claims that the DD value of chitosan indicated the extent of bacterial growth inhibition and that only a soluble fraction of chitosan films demonstrated antibacterial activity. The chitosan films fully suppressed the development of Gram-negative (*E. coli*) bacteria with a 90% DD. The degree of bacterial viability was established by the duration of the cells' interaction with the film surfaces. All bacterial strains' live cells were undetectable using the agar diffusion method after 24 h of contact with chitosan films, and minimal inactivation was observed after 1 h of cell incubation on the film surface. Nonetheless, the antibacterial activity of chitosan films is still up for debate.

Karthikeyan et al. [34] and Guan et al. [98] provide the following explanation and become the basis for explaining the film chit-PVA-cur-capped ZnO-CuO NPs' antibacterial activity. When bacteria were exposed to the composite film, their cell walls and membranes lost their structural integrity, and their regular physiological processes were unstable. The contact between the bacterial cells and the film chit-PVA-cur-capped ZnO-CuO NPs is depicted in Fig. 16. This contact can weaken the integrity of the cell membrane and change the structures of macromolecules such as proteins, lipids, and DNA. The bacterial cell membrane is negatively charged, while the Zn^{2+} ion and Cu^{2+} are positively charged due to the interaction of both systems.

A greater surface area, asymmetrical external ridges, and electrostatic attraction as the chit-PVA-cur-capped ZnO-CuO NPs film pierces the cell membrane are some of these physical and chemical characteristics. It also greatly stimulates the release of Zn^{2+} and Cu^{2+} ions, which can cause oxidative stress in the bacterial cell and the generation of reactive oxygen species (ROS), as well as increases in oxygen vacancies and the molecules' ability to diffuse (chitosan, PVA, and curcumin). Finally, ROS such H_2O_2, $O_2\bullet^-$, $OH\bullet^-$, Cu^{2+}, and Zn^{2+} attach to the cell membrane's negative surface, rupturing the cells and allowing cellular material to escape, which eventually leads to cell death [75].

The results of the FTIR film analysis [97,99] demonstrated that interactions between PVA and chitosan involve both electrostatic and hydrogen bonding within and between the chains of both polymers. The enhanced antibacterial activity of the films is most likely due to these interactions as well as the higher concentration of cur-capped ZnO-CuO NPs compared to one-component films. Data from SEM-EDS can explain the antibacterial properties of a sample [100]. It is further explained that the metal ion content detected in SEM-EDS functions as an antibacterial.

■ CONCLUSION

Cur-capped ZnO-CuO NPs resulting from biosynthesis have particle sizes and polydispersity indexes of 485.24 ± 5.66 nm and 0.688 ± 0.540, respectively. The maximum wavelength of cur-capped ZnO-CuO NPs is 460 nm. The chit-PVA-cur-capped ZnO-CuO NPs film has a thickness of 0.17 to 0.30 mm, a moisture content of 9.09 to 10.00% and a swelling degree of 140 to 200% but decreased water-soluble matter from 50 to 20%. The Zn–O and Cu–O functional groups in cur-capped ZnO-CuO NPs were detected at 482–426 and 603 cm^{-1}, respectively. The Zn–O and Cu–O groups in all chi-PVA-cur-capped ZnO-CuO NPs films were detected at 424–475 and 584–619 cm^{-1}, respectively. The crystallinity size of cur-capped ZnO-

CuO NPs is 5.72 nm. All films of chit-PVA-cur-capped ZnO-CuO NPs had an amorphous form. The surface morphology of all chit-PVA-cur-capped ZnO-CuO NPs films was dense, homogeneous, and slightly rough. The results of the *E. coli* antibacterial test of the chit-PVA-cur-capped ZnO-CuO NPs type C film had a larger inhibition zone than the type A and B films. Based on the synthesis of chi-PVA-cur-capped ZnO-CuO NPs films, the studies conclude that these composite films are successful and can be suggested as multifunctional materials with high potential for antibacterial, food packaging, and biomedical applications.

■ ACKNOWLEDGMENTS

Thank you to *Direktorat Penelitian Dan Pengabdian Kepada Masyarakat, Direktorat Jenderal Riset Dan Pengembangan, Kementerian Pendidikan Tinggi, Sains dan Teknologi* for funding this research (*Hibah Penelitian Fundamental-Reguler*, No. 175/LL2/AL.04.03/PL-BARU/2026).

■ CONFLICT OF INTEREST

State that all the authors have no conflict of interest related to this manuscript.

■ AUTHOR CONTRIBUTIONS

Ahmad Fatoni, Nabila Wulandari, and Hilma conducted the experiment. Ahmad Fatoni and Nurlisa Hidayati conducted the interpretation of data from UV-vis spectra, FTIR spectra, particle sizes, polydispersity index analysis, XRD diffractogram, SEM, and antibacterial test. Ahmad Fatoni wrote and revised the manuscript. All authors agreed to the final version of this manuscript.

■ REFERENCES

[1] Saravanan, A., Kumar, P.S., Karishma, S., Vo, D.V.N., Jeevanantham, S., Yaashikaa, P.R., and George, C.S., 2021, A review on biosynthesis of metal nanoparticles and its environmental applications, *Chemosphere*, 264, 128580.

[2] Khan, I., Saeed, K., and Khan, I., 2019, Nanoparticles: Properties, applications and toxicities, *Arabian J. Chem.*, 12 (7), 908–931.

[3] Nyabadza, A., McCarthy, É., Makhesana, M., Heidarinassab, S., Plouze, A., Vazquez, M., and Brabazon, D., 2023, A review of physical, chemical and biological synthesis methods of bimetallic nanoparticles and applications in sensing, water treatment, biomedicine, catalysis and hydrogen storage, *Adv. Colloid Interface Sci.*, 321, 103010.

[4] Yazdani, Z., Mehrgan, M.S., Khayatzadeh, J., Shekarabi, S.P.H., and Tabrizi, M.H., 2023, Dietary green-synthesized curcumin-mediated zinc oxide nanoparticles promote growth performance, haemato-biochemical profile, antioxidant status, immunity, and carcass quality in Nile tilapia (*Oreochromis niloticus*), *Aquacult. Rep.*, 32, 101717.

[5] Jayarambabu, N., Akshaykranth, A., Venkatappa Rao, T., Venkateswara Rao, K., and Rakesh Kumar, R., 2020, Green synthesis of Cu nanoparticles using *Curcuma longa* extract and their application in antimicrobial activity, *Mater. Lett.*, 259, 126813.

[6] Faisal, S., Al-Radadi, N.S., Jan, H., Abdullah, A., Shah, S.A., Shah, S., Rizwan, M., Afsheen, Z., Hussain, Z., Uddin, M.N., Idrees, M., and Bibi, N., 2021, *Curcuma longa* mediated synthesis of copper oxide, nickel oxide and Cu-Ni bimetallic hybrid nanoparticles: Characterization and evaluation for antimicrobial, anti-parasitic and cytotoxic potentials, *Coatings*, 11 (7), 849.

[7] Patra, D., and El Kurdi, R., 2021, Curcumin as a novel reducing and stabilizing agent for the green synthesis of metallic nanoparticles, *Green Chem. Lett. Rev.*, 14 (3), 474–487.

[8] Hao, Z., Wang, M., Cheng, L., Si, M., Feng, Z., and Feng, Z., 2024, Synergistic antibacterial mechanism of silver-copper bimetallic nanoparticles, *Front. Bioeng. Biotechnol.*, 11, 1337543.

[9] Padilla-Cruz, A.L., Garza-Cervantes, J.A., Vasto-Anzaldo, X.G., García-Rivas, G., León-Buitimea, A., and Morones-Ramírez, J.R., 2021, Synthesis and design of Ag–Fe bimetallic nanoparticles as antimicrobial synergistic combination therapies against clinically relevant pathogens, *Sci. Rep.*, 11 (1), 5351.

[10] Xaviour, J., Sreelekshmi, S., Joseph, J., Fathima, S.A.,

and Sajini, T., 2024, Eco-friendly synthesis and enhanced antibacterial action of bimetallic Ag/ZnO nanoparticles using *Hylocereus costaricensis* stem extract, *RSC Sustainability*, 2 (10), 3077–3089.

[11] Cirillo, G., Curcio, M., Oliviero Rossi, C., De Filpo, G., Baratta, M., De Luca, M., Iemma, F., and Nicoletta, F.P., 2023, Curcumin–sodium alginate and curcumin–chitosan conjugates as drug delivery systems: An interesting rheological behaviour, *Molecules*, 28 (15), 5893.

[12] Pourbagher, H., Sharifzadeh, B., Golsefidi, M.A., and Mirmasoudi, S.S., 2024, Evaluation of drug delivery performance of curcumin by chitosan synthesized from the skin of the shrimp of the Gulf of Gorgan, *Next Nanotechnol.*, 6, 100085.

[13] O'Toole, M.G., Soucy, P.A., Chauhan, R., Raju, M.V.R., Patel, D.N., Nunn, B.M., Keynton, M.A., Ehringer, W.D., Nantz, M.H., Keynton, R.S., and Gobin, A.S., 2016, Release-modulated antioxidant activity of a composite curcumin-chitosan polymer, *Biomacromolecules*, 17 (4), 1253–1260.

[14] Liu, Y., Liu, D., Zhu, L., Gan, Q., and Le, X., 2015, Temperature-dependent structure stability and *in vitro* release of chitosan-coated curcumin liposome, *Food Res. Int.*, 74, 97–105.

[15] Saranya, T.S., Rajan, V.K., Biswas, R., Jayakumar, R., and Sathianarayanan, S., 2018, Synthesis, characterisation and biomedical applications of curcumin conjugated chitosan microspheres, *Int. J. Biol. Macromol.*, 110, 227–233.

[16] Wu, C., Sun, J., Chen, M., Ge, Y., Ma, J., Hu, Y., Pang, J., and Yan, Z., 2019, Effect of oxidized chitin nanocrystals and curcumin into chitosan films for seafood freshness monitoring, *Food Hydrocolloids*, 95, 308–317.

[17] Ahmed Ismail, K., El Askary, A., Farea, M.O., Awwad, N.S., Ibrahium, H.A., Eid Moustapha, M., and Menazea, A.A., 2022, Perspectives on composite films of chitosan-based natural products (ginger, curcumin, and cinnamon) as biomaterials for wound dressing, *Arabian J. Chem.*, 15 (4), 103716.

[18] Jogaiah, S., Mujtaba, A.G., Mujtaba, M., Archana, A., De Britto, S., Geetha, N., Belorkar, S.A., and Shetty, H.S., 2025, Chitosan-metal and metal oxide nanocomposites for active and intelligent food packaging; A comprehensive review of emerging trends and associated challenges, *Carbohydr. Polym.*, 357, 123459.

[19] Fatoni, A., Rendowati, A., Sirumapea, L., Miranti, L., Masitoh, S., and Hidayati, N., 2023, Synthesis, characterization of chitosan-ZnO/CuO nanoparticles film, and its effect as an antibacterial agent of *Escherichia coli*, *Sci. Technol. Indones.*, 8 (3), 373–381.

[20] Güldiken, Ç.G., Karaosmanoğlu, O., Sivas, H., and Gerçel, H.F., 2020, ZnO microparticle-loaded chitosan/poly(vinyl alcohol)/acacia gum nanosphere-based nanocomposite thin film wound dressings for accelerated wound healing, *J. Appl. Polym. Sci.*, 137 (10), 48445.

[21] Gutha, Y., Pathak, J.L., Zhang, W., Zhang, Y., and Jiao, X., 2017, Antibacterial and wound healing properties of chitosan/poly(vinyl alcohol)/zinc oxide beads (CS/PVA/ZnO), *Int. J. Biol. Macromol.*, 103, 234–241.

[22] Jahan, F., Mathad, R.D., and Farheen, S., 2016, Effect of mechanical strength on chitosan-PVA blend through ionic crosslinking for food packaging application, *Mater. Today: Proc.*, 3 (10, Pt. B), 3689–3696.

[23] Grande-Tovar, C.D., Castro Castro, J.I., Barba-Rosado, L.V., Zapata, P.A., Insuasty, D., and Valencia-Llano, C.H., 2025, Histology assessment of chitosan–polyvinyl alcohol scaffolds incorporated with CaO nanoparticles, *Molecules*, 30 (2), 276.

[24] Islam, F., Rahman, E., Tarannum, T., and Islam, N., 2024, Assessment of chitosan-PVA hydrogels infused with marine collagen peptides for potential wound healing applications, *Compos., Part C: Open Access*, 15, 100528.

[25] Momtaz, F., Momtaz, E., Mehrgardi, M.A., Momtaz, M., Narimani, T., and Poursina, F., 2024, Enhanced antibacterial properties of polyvinyl alcohol/starch/chitosan films with NiO–CuO nanoparticles for food packaging, *Sci. Rep.*, 14 (1), 7356.

[26] Gobi, R., and Babu, R.S., 2025, *In-vitro* investigation of chitosan/polyvinyl alcohol/TiO_2 composite membranes for wound regeneration, *Biochem. Biophys. Res. Commun.*, 742, 151129.

[27] Khisore, M., Hussein, S.A.M., Abdoon, F.M., Bindu, G.N.H., Hamad, A.A., Saxena, K.K., Raj, R.G., Kumar, A., and Srinivas, T., 2025, Chitosan–PVA composite reinforced with Cu-decorated ZnO nanoparticles for photocatalytic dye degradation, *Chem. Phys. Impact*, 11, 100953.

[28] Abbas, M., Hussain, T., Arshad, M., Ansari, A.R., Irshad, A., Nisar, J., Hussain, F., Masood, N., Nazir, A., and Iqbal, M., 2019, Wound healing potential of curcumin cross-linked chitosan/polyvinyl alcohol, *Int. J. Biol. Macromol.*, 140, 871–876.

[29] Niranjan, R., Kaushik, M., Prakash, J., Venkataprasanna, K.S., Arpana, C., Balashanmugam, P., and Venkatasubbu, G.D., 2019, Enhanced wound healing by PVA/chitosan/curcumin patches: *In vitro* and *in vivo* study, *Colloids Surf., B*, 182, 110339.

[30] Khezri, A., Karimi, A., Yazdian, F., Jokar, M., Mofradnia, S.R., Rashedi, H., and Tavakoli, Z., 2018, Molecular dynamic of curcumin/chitosan interaction using a computational molecular approach: Emphasis on biofilm reduction, *Int. J. Biol. Macromol.*, 114, 972–978.

[31] Venkatas, J., Daniels, A., and Singh, M., 2022, The potential of curcumin-capped nanoparticle synthesis in cancer therapy: A green synthesis approach, *Nanomaterials,* 12 (18), 3201.

[32] El-Kattan, N., Emam, A.N., Mansour, A.S., Ibrahim, M.A., Abd El-Razik, A.B., Allam, K.A.M., Riad, N.Y., and Ibrahim, S.A., 2022, Curcumin assisted green synthesis of silver and zinc oxide nanostructures and their antibacterial activity against some clinical pathogenic multi-drug resistant bacteria, *RSC Adv.*, 12 (28), 18022–18038.

[33] Arab, C., El Kurdi, R., and Patra, D., 2021, Chitosan coated zinc curcumin oxide nanoparticles for the determination of ascorbic acid, *J. Mol. Liq.*, 328, 115504.

[34] Karthikeyan, C., Varaprasad, K., Akbari-Fakhrabadi, A., Hameed, A.S.H., and Sadiku, R., 2020, Biomolecule chitosan, curcumin and ZnO-based antibacterial nanomaterial, via a one-pot process, *Carbohydr. Polym.*, 249, 116825.

[35] Sutharsan, J., Boyer, C.A., and Zhao, J., 2022, Physicochemical properties of chitosan edible films incorporated with different classes of flavonoids, *Carbohydr. Polym. Technol. Appl.*, 4, 100232.

[36] Oluwasina, O.O., Akinyele, B.P., Olusegun, S.J., Oluwasina, O.O., and Mohallem, N.D.S., 2021, Evaluation of the effects of additives on the properties of starch-based bioplastic film, *SN Appl. Sci.*, 3 (4), 421.

[37] Isnaeni, I., Hendradi, E., and Zettira, N.Z., 2020, Inhibitory effect of roselle aqueous extracts-HPMC 6000 gel on the growth of *Staphylococcus aureus* ATCC 25923, *Turk. J. Pharm. Sci.*, 17 (2), 190–196.

[38] Alallam, B., Doolaanea, A.A., Alfatama, M., and Lim, V., 2023, Phytofabrication and characterisation of zinc oxide nanoparticles using pure curcumin, *Pharmaceuticals*, 16 (2), 269.

[39] Elattar, K.M., Ghoniem, A.A., Al-Otibi, F.O., Fakhouri, A.S., Helmy, Y.A., Saber, W.E.I.A., Hassan, M.A.E., and Elsayed, A., 2025, Eco-friendly synthesis of Ag/CeO_2 and CuO/CeO_2 nanocomposites using Curcuma longa extract and assessment of their antioxidant, antifungal, and cytotoxic activities, *RSC Adv.*, 15 (16), 12100–12116.

[40] Moussawi, R.N., and Patra, D., 2016, Modification of nanostructured ZnO surfaces with curcumin: Fluorescence-based sensing for arsenic and improving arsenic removal by ZnO, *RSC Adv.*, 6 (21), 17256–17268.

[41] Khor, P.Y., Mohd Aluwi, M.F.F., Rullah, K., and Lam, K.W., 2019, Insights on the synthesis of asymmetric curcumin derivatives and their biological activities, *Eur. J. Med. Chem.*, 183, 111704.

[42] Prasad, S., DuBourdieu, D., Srivastava, A., Kumar, P., and Lall, R., 2021, Metal–curcumin complexes in therapeutics: An approach to enhance pharmacological effects of curcumin, *Int. J. Mol. Sci.*, 22 (13), 7094.

[43] Xu, J., Zhang, Y., Gutha, Y., and Zhang, W., 2017, Antibacterial property and biocompatibility of chitosan/poly(vinyl alcohol)/ZnO (CS/PVA/ZnO) beads as an efficient adsorbent for Cu(II) removal from aqueous solution, *Colloids Surf., B*, 156, 340–348.

[44] Mirzaeei, S., Taghe, S., Asare-Addo, K., and Nokhodchi, A., 2021, Polyvinyl alcohol/chitosan single-layered and polyvinyl alcohol/chitosan/Eudragit RL100 multi-layered electrospun nanofibers as an ocular matrix for the controlled release of ofloxacin: An *in vitro* and *in vivo* evaluation, *AAPS PharmSciTech*, 22 (5), 170.

[45] Alotaibi, B.S., Khan, A.K., Kharaba, Z., Yasin, H., Yasmin, R., Ijaz, M., Khan, M., and Murtaza, G., 2024, Development of poly(vinyl alcohol)-chitosan composite nanofibers for dual drug therapy of wounds, *ACS Omega*, 9 (11), 12825–12834.

[46] Madian, N.G., El-Ashmanty, B.A., and Abdel-Rahim, H.K., 2023, Improvement of chitosan films properties by blending with cellulose, honey and curcumin, *Polymers*, 15 (12), 2587.

[47] Ahmad, A.A., and Sarbon, N.M., 2021, A comparative study: Physical, mechanical and antibacterial properties of bio-composite gelatin films as influenced by chitosan and zinc oxide nanoparticles incorporation, *Food Biosci.*, 43, 101250.

[48] Dordevic, S., Dordevic, D., Tesikova, K., Sedlacek, P., Kalina, M., Vapenka, L., Nejezchlebova, M., Treml, J., Tremlova, B., and Koudelková Mikulášková, H., 2024, Nanometals incorporation into active and biodegradable chitosan films, *Heliyon*, 10 (7), e28430.

[49] Abdeen, Z.I., El Farargy, A.F., and Negm, N.A., 2018, Nanocomposite framework of chitosan/polyvinyl alcohol/ZnO: Preparation, characterization, swelling and antimicrobial evaluation, *J. Mol. Liq.*, 250, 335–343.

[50] Liang, Q., Jiang, L., Zheng, J., and Duan, N., 2024, Determination of high concentration copper ions based on ultraviolet—visible spectroscopy combined with partial least squares regression analysis, *Processes*, 12 (7), 1408.

[51] Le, Q.H., Friebe, C., Wang, W.C., and Wondraczek, L., 2019, Spectroscopic properties of Cu^{2+} in alkaline earth metaphosphate, fluoride-phosphate and fluoride-phosphate-sulfate glasses, *J. Non-Cryst. Solids: X*, 4, 100037.

[52] Dangana, R.S., George, R.C., Shittu, U.O., and Agboola, F.K., 2023, Facile biosynthesis, characterisation and biotechnological application of ZnO nanoparticles mediated by leaves of *Cnidoscolus aconitifolius*, *Artif. Cells, Nanomed., Biotechnol.*, 51 (1), 309–317.

[53] Ahmad, T., Waheed, A., Abdel-Azeim, S., Khan, S., and Ullah, S., 2022, Three new turn-on fluorescent sensors for the selective detection of Zn^{2+}: Synthesis, properties and DFT studies, *Arabian J. Chem.*, 15 (8), 104002.

[54] Kubler, J.A., Pfund, B., and Wenger, O.S., 2022, Zinc(II) complexes with triplet charge-transfer excited states enabling energy-transfer catalysis, photoinduced electron transfer, and upconversion, *JACS Au*, 2 (10), 2367–2380.

[55] Muniyappan, N., Pandeeswaran, M., and Amalraj, A., 2021, Green synthesis of gold nanoparticles using *Curcuma pseudomontana* isolated curcumin: Its characterization, antimicrobial, antioxidant and anti- inflammatory activities, *Environ. Chem. Ecotoxicol.*, 3, 117–124.

[56] Lu, C., Yao, Z., Feng, J., Mao, B., and Jin, G., 2023, Oil-in-water strategy coating curcumin-nido-carborane fluorescent complex with acrylic resins for cell imaging, *Arabian J. Chem.*, 16 (8), 104876.

[57] El-Kattan, N., Ibrahim, M.A., Emam, A.N., Metwally, K., Youssef, F.S., Nassar, N.A., and Mansour, A.S., 2025, Evaluation of the antimicrobial activity of chitosan- and curcumin-capped copper oxide nanostructures against multi-drug-resistant microorganisms, *Nanoscale Adv.*, 7 (10), 2988–3007.

[58] Soumya, K.R., Snigdha, S., Sugathan, S., Mathew, J., and Radhakrishnan, E.K., 2017, Zinc oxide–curcumin nanocomposite loaded collagen membrane as an effective material against

methicillin-resistant coagulase-negative Staphylococci, *3 Biotech*, 7 (4), 238.

[59] Saif, A., Omer, M.O., Sattar, A., Tipu, Y., Alharbi, H.M., Saher, U., and Awan, T., 2024, Comprehensive analysis of curcumin zinc oxide nanoparticles, synthesis, characterization, and cytogenotoxic profiling, *ACS Omega*, 9 (26), 28186–28193.

[60] Kalirajan, C., and Palanisamy, T., 2019, A ZnO-curcumin nanocomposite embedded hybrid collagen scaffold for effective scarless skin regeneration in acute burn injury, *J. Mater. Chem. B*, 7 (38), 5873–5886.

[61] Faham, S., Ghavami, R., Golmohammadi, H., and Khayatian, G., 2019, Spectrophotometric and visual determination of zoledronic acid by using a bacterial cell-derived nanopaper doped with curcumin, *Microchim. Acta*, 186 (11), 719.

[62] Enumo, A., Argenta, D.F., Bazzo, G.C., Caon, T., Stulzer, H.K., and Parize, A.L., 2020, Development of curcumin-loaded chitosan/pluronic membranes for wound healing applications, *Int. J. Biol. Macromol.*, 163, 167–179.

[63] Prateeksha, P., Rao, C.V., Das, A.K., Barik, S.K., and Singh, B.N., 2019, ZnO/curcumin nanocomposites for enhanced inhibition of *Pseudomonas aeruginosa* virulence via LasR-RhlR quorum sensing systems, *Mol. Pharmaceutics*, 16 (8), 3399–3413.

[64] Qasem, M., El Kurdi, R., and Patra, D., 2020, Green Synthesis of curcumin conjugated CuO nanoparticles for catalytic reduction of methylene blue, *ChemistrySelect*, 5 (5), 1694–1704.

[65] Madeo, L.F., Schirmer, C., Cirillo, G., Froeschke, S., Hantusch, M., Curcio, M., Nicoletta, F.P., Büchner, B., Mertig, M., and Hampel, S., 2023, Facile one-pot hydrothermal synthesis of a zinc oxide/curcumin nanocomposite with enhanced toxic activity against breast cancer cells, *RSC Adv.*, 13 (39), 27180–27189.

[66] Zidan, H.M., Abdelrazek, E.M., Abdelghany, A.M., and Tarabiah, A.E., 2019, Characterization and some physical studies of PVA/PVP filled with MWCNTs, *J. Mater. Res. Technol.*, 8 (1), 904–913.

[67] Ewais, A., Saber, R.A., Abdel Ghany, A., Sharaf, A., and Sitohy, M., 2023, High quality, low molecular weight shrimp and crab chitosans obtained by short-time holistic high-power microwave technology, *SN Appl. Sci.*, 5 (12), 365.

[68] da Silva, R.S.M., Barbosa, R.C., dos Santos Chagas, C., da Silva, E.B., Feder, D., Fonseca, F.L.A., and Fook, M.V.L., 2022, Development, preparation and characterization of chitosan, gelatin and heparin membranes for biomedical applications, *SN Appl. Sci.*, 4 (2), 44.

[69] Al Kiey, S.A., Toderaș, M., Al-Qabandi, O.A., Bassyouni, M., Zhou, Q., El Fray, M., and Hasanin, M.S., 2024, Investigating the hybrid potential of PVA-chitosan-loaded TiO_2@NiO films for advanced conductivity and dielectric performance, *Polym. Test.*, 138, 108546.

[70] Correa-Pacheco, Z.N., Bautista-Baños, S., Hernández-López, M., Tapia-Maruri, D., Jiménez-Pérez, J.L., Ortega-Gudiño, P., and Cruz-Miranda, O.L., 2025, Characterization of nanostructured chitosan-PVA films and their effects on blueberries during storage, *Future Foods*, 11, 100571.

[71] Ribas, M.M., Aguiar, G.P.S., Muller, L.G., Siebel, A.M., Lanza, M., and Oliveira, J.V., 2019, Curcumin-nicotinamide cocrystallization with supercritical solvent (CSS): Synthesis, characterization and *in vivo* antinociceptive and anti-inflammatory activities, *Ind. Crops Prod.*, 139, 111537.

[72] Mailafiya, M.M., Abubakar, K., Danmaigoro, A., Chiroma, S.M., Rahim, E.B.A., Moklas, M.A.M., and Zakaria, Z.A.B., 2019, Evaluation of *in vitro* release kinetics and mechanisms of curcumin-loaded cockle shell-derived calcium carbonate nanoparticles, *Biomed. Res. Ther.*, 6 (12), 3518–3540.

[73] Kabiriyel, J., Jeyanthi, R., Jayakumar, K., Amalraj, A., Arjun, P., Shanmugarathinam, A., Vignesh, G., and Mohan, C.R., 2023, Green synthesis of carboxy methyl chitosan based curcumin nanoparticles and its biological activity: Influence of size and conductivity, *Carbohydr. Polym. Technol. Appl.*, 5, 100260.

[74] Wijayawardana, S., Thambiliyagodage, C., and Jayanetti, M., 2024, Kinetic study of *in vitro* release

of curcumin from chitosan biopolymer and the evaluation of biological efficacy, *Arabian J. Chem.*, 17 (9), 105896.

[75] Perera, W.P.T.D., Dissanayake, R.K., Ranatunga, U.I., Hettiarachchi, N.M., Perera, K.D.C., Unagolla, J.M., De Silva, R.T., and Pahalagedara, L.R., 2020, Curcumin loaded zinc oxide nanoparticles for activity-enhanced antibacterial and anticancer applications, *RSC Adv.*, 10 (51), 30785–30795.

[76] Sayyar, Z., and Jafarizadeh Malmiri, H., 2019, Photocatalytic and antibacterial activities study of prepared self-cleaning nanostructure surfaces using synthesized and coated ZnO nanoparticles with curcumin nanodispersion, *Z. Kristallogr. - Cryst. Mater.*, 234 (5), 307–328.

[77] Kamble, S., Utage, B., Mogle, P., Kamble, R., Hese, S., Dawane, B., and Gacche, R., 2016, Evaluation of curcumin capped copper nanoparticles as possible inhibitors of human breast cancer cells and angiogenesis: A comparative study with native curcumin, *AAPS PharmSciTech*, 17 (5), 1030–1041.

[78] Kumar, S., Krishnakumar, B., Sobral, A.J.F.N., and Koh, J., 2019, Bio-based (chitosan/PVA/ZnO) nanocomposites film: Thermally stable and photoluminescence material for removal of organic dye, *Carbohydr. Polym.*, 205, 559–564.

[79] Varaprasad, K., López, M., Núñez, D., Jayaramudu, T., Sadiku, E.R., Karthikeyan, C., and Oyarzúnc, P., 2020, Antibiotic copper oxide-curcumin nanomaterials for antibacterial applications, *J. Mol. Liq.*, 300, 112353.

[80] Kalpana, V.N., Kataru, B.A.S., Sravani, N., Vigneshwari, T., Panneerselvam, A., and Devi Rajeswari, V., 2018, Biosynthesis of zinc oxide nanoparticles using culture filtrates of *Aspergillus niger*: Antimicrobial textiles and dye degradation studies, *OpenNano*, 3, 48–55.

[81] Cao, Y., Dhahad, H.A., El-Shorbagy, M.A., Alijani, H.Q., Zakeri, M., Heydari, A., Bahonar, E., Slouf, M., Khatami, M., Naderifar, M., Iravani, S., Khatami, S., and Dehkordi, F.F., 2021, Green synthesis of bimetallic ZnO–CuO nanoparticles and their cytotoxicity properties, *Sci. Rep.*, 11 (1), 23479.

[82] Sathiyabama, M., Indhumathi, M., and Amutha, T., 2020, Preparation and characterization of curcumin functionalized copper nanoparticles and their application enhances disease resistance in chickpea against wilt pathogen, *Biocatal. Agric. Biotechnol.*, 29, 101823.

[83] Al-Khezraji, A.A.R., Abd Ali, H.R., Yousif, A.A., and Abed, H.R., 2021, Effect of mixed ZnO/CuO nanoparticles on the structural, morphological, and topographical properties, *J. Phys.: Conf. Ser.*, 1963 (1), 012053.

[84] Teklu, B., Kadiri, S.K., and Vidavalur, S., 2023, Green synthesis of copper oxide nanoparticles using *Balanites aegyptiaca* stem bark extract and investigation of antibacterial activity, *Results Chem.*, 6, 101152.

[85] More, D.S., Moloto, M.J., Moloto, N., and Matabola, K.P., 2021, Silver/copper nanoparticle-modified polymer chitosan/PVA blend fibers, *Int. J. Polym. Sci.*, 2021 (1), 6217609.

[86] Abdullah, H., Naqvi, S.A.R., Xiao, F., Nazir, M.S., Sun, Y., Rafique, A., Lodhi, N.A., and Ul Hassan, S., 2025, Biomedical frontiers with PVA–chitosan/lignin@CdZnO multifunctional hydrogel, *RSC Adv.*, 15 (40), 33682–33694.

[87] Rajendran, D., Shobha, M., Mohana, S., Gopi, M., Ramachandran, N., Franklin, M.E.E., Manimaran, A., Huliyurdurga Shameeulla, H., Selvaraju, S., and Sahoo, A., 2025, Comprehensive characterization and biological and safety evaluation of zinc oxide-curcumin nanoconjugates: unraveling synergistic effects for enhanced therapeutic applications, *ACS Omega*, 10 (25), 27045–27057.

[88] Liu, Y., Cai, Y., Jiang, X., Wu, J., and Le, X., 2016, Molecular interactions, characterization and antimicrobial activity of curcumin–chitosan blend films, *Food Hydrocolloids*, 10, 27045–27057.

[89] Olewnik-Kruszkowska, E., Gierszewska, M., Jakubowska, E., Tarach, I., Sedlarik, V., and Pummerova, M., 2019, Antibacterial films based on PVA and PVA–chitosan modified with poly(hexamethylene guanidine), *Polymers*, 11 (12), 2093.

[90] Alrobea, H., Khan, A., Alamry, K.A., and Hussein, M.A., 2024, Antibacterial evaluation of polyvinyl alcohol/polyvinyl pyrrolidone/chitosan nanocomposite embedded curcumin@zinc oxide, *Results Chem.*, 10, 101729.

[91] Iswarya, S., Bharathi, M., Hariram, N., Theivasanthi, T., and Gopinath, S.C.B., 2024, Solid polymer electrolyte and antimicrobial performance of polyvinyl alcohol/silver nanoparticles composite film, *Results Chem.*, 7, 101431.

[92] Hu, D., Wang, H., and Wang, L., 2016, Physical properties and antibacterial activity of quaternized chitosan/carboxymethyl cellulose blend films, *LWT-Food Sci. Technol.*, 65, 398–405.

[93] Raafat, D., and Sahl, H.G., 2009, Chitosan and its antimicrobial potential - A critical literature survey, *Microb. Biotechnol.*, 2 (2), 186–201.

[94] Rabea, E.I., Badawy, M.E.T., Stevens, C.V., Smagghe, G., and Steurbaut, W., 2003, Chitosan as antimicrobial agent: Applications and mode of action, *Biomacromolecules*, 4 (6), 1457–1465.

[95] Foster, L.J.R., and Butt, J., 2011, Chitosan films are NOT antimicrobial, *Biotechnol. Lett.*, 33 (2), 417–421.

[96] Rodríguez-Núñez, J.R., Madera-Santana, T.J., Sánchez-Machado, D.I., López-Cervantes, J., and Soto Valdez, H., 2014, Chitosan/hydrophilic plasticizer-based films: Preparation, physicochemical and antimicrobial properties, *J. Polym. Environ.*, 22 (1), 41–51.

[97] Malinowska-Pańczyk, E., Staroszczyk, H., Gottfried, K., Kołodziejska, I., and Wojtasz-Pająk, A., 2015, Antimicrobial properties of chitosan solutions, chitosan films and gelatin-chitosan films, *Polimery*, 60 (11-12), 735–741.

[98] Guan, G., Zhang, L., Zhu, J., Wu, H., Li, W., and Sun, Q., 2021, Antibacterial properties and mechanism of biopolymer-based films functionalized by CuO/ZnO nanoparticles against *Escherichia coli* and *Staphylococcus aureus*, *J. Hazard. Mater.*, 402, 123542.

[99] Staroszczyk, H., Sztuka, K., Wolska, J., Wojtasz-Pająk, A., and Kołodziejska, I., 2013, Interactions of fish gelatin and chitosan in uncrosslinked and crosslinked with EDC films: FT-IR study, *Spectrochim. Acta, Part A*, 117, 707–712.

[100] Aziz, I., Mulyani, E., and Yusuf, Y., 2023, Morphological, mechanical and antibacterial properties of Ti–Cu–N thin films deposited by sputtering DC, *Heliyon*, 9 (6), e17170.